# Design and Analysis of a Dual Rotor Multiphase Brushless DC Motor for its Application in Electric Vehicles

Mujtaba Hussain
Department of Electrical Power Engineering
U.S.-Pakistan Center for Advanced Studies in Energy
National University of Sciences and Technology
Islamabad, Pakistan
mujtaba.hussein@gmail.com

Abasin Ulasyar
Department of Electrical Power Engineering
U.S.-Pakistan Center for Advanced Studies in Energy
National University of Sciences and Technology
Islamabad, Pakistan
abasin@uspcase.nust.edu.pk

Haris Sheh Zad
Department of Mechanical & Manufacturing Engineering
Pak-Austria Fachhochshule Institute of Applied Sciences and Technology
Haripur, Pakistan
haris.shehzad@fcm3.paf-iast.edu.pk

Abraiz Khattak
Department of Electrical Power Engineering
U.S.-Pakistan Center for Advanced Studies in Energy
National University of Sciences and Technology
Islamabad, Pakistan
abraiz@uspcase.nust.edu.pk

Shibli Nisar
Military College of Signals
National University of Sciences and Technology
Islamabad, Pakistan
shiblinisar@mcs.edu.pk

Kashif Imran
Department of Electrical Power Engineering
U.S.-Pakistan Center for Advanced Studies in Energy
National University of Sciences and Technology
Islamabad, Pakistan
kashifimran@uspcase.nust.edu.pk

**Abstract-The main objective of this paper is to study the effect of phase numbers in the dual rotor Brushless DC (BLDC) motor for its application in Electric Vehicles (EVs). The performance of two novel 5-, and 7-phase dual rotor BLDC motors is compared against the standard 3-phase dual rotor BLDC motor. The proposed motors combine the positive characteristics of multiphase BLDC motor and the dual rotor BLDC motor thus achieving better fault tolerance capability, high power density, and less per phase stator current. Finite Element Method (FEM) was used to design the 3-, 5-, and 7-phase dual-rotor BLDC motors. The design parameters and operating conditions are kept the same for a fair comparison. The stator current and torque performance of the proposed motors were obtained with FEM simulation and were compared with the standard 3-phase dual rotor BLDC motor. It is possible to use low power rating power electronics switches for the proposed motor. The simulation results also validate low torque ripples and high-power density in the proposed motors. Finally, the fault analysis of the designed motors shows that the fault tolerance capability increases as the phase number increases.**

***Keywords-dual rotor; Brushless DC (BLDC); Electric Vehicle (EV); multiphase; Finite Element Method (FEM)***

## I. INTRODUCTION

Electric Vehicles (EVs) are the future of road transportation. Extensive research has been conducted on the drive system of EVs to provide low-cost and energy-efficient solutions. The electric motor is an integral part of its propulsion system along with the transmission system, the power electronics, and the battery [1]. The basic requirements of the electric motor for EV applications include high torque and power density, varied speed range (high speed cruising and low speed crawling), high efficiency over wide torque and speed ranges, wide constant power operation region, high intermittent overload capability, and high reliability and robustness [2-6]. The main advantages of the Brushless DC (BLDC) motor are its small size, the absence of rotor copper losses due to yhe absence of rotor windings, and its low maintenance cost [7]. The BLDC motor offers high efficiency, high power, and torque density, but the conventional BLDC motor topologies do not provide all the requirements for EV application [8-10].

The dual-rotor BLDC machine promises high torque density and high efficiency. This motor consists of an outer rotor, an inner rotor, and a stator between them. In other words, two separate motors share the same stator nested between them

Corresponding author: Abasin Ulasyar

[11-12]. Since both sides of the stator are used as compared to single rotor Permanent Magnet (PM) BLDC, this structure improves the torque density. The topology reduces the copper quantity, which in turn reduces the winding resistance. Thus, the copper losses are reduced, and efficiency is improved. The reduced copper usage also cuts down the cost [13-15].

The next important requirement for PM BLDC machines used in EV applications is fault tolerance which is the ability of a system to continue working even if a fault occurs. The fault-tolerant capability of the PM BLDC motors can be enhanced by increasing the number of stator phases (more than three-phase). In a multiphase PM BLDC drive system, increasing the phase number also increases the number of power electronic switches while it reduces the converter rating required per phase [16-17]. The multiphase PM BLDC motors have low torque ripple and high torque density as compared to the three-phase electric motors [18-20]. It is now evident that dual-rotor PM BLDC and multiphase PM BLDC topologies offer unique advantages for EV application. These two topologies can be combined to get the positive characteristics of multiphase PM BLDC machines and dual-rotor PM BLDC machines.

In our research work, two dual rotor BLDC motors with 5, and 7 phases are designed for EV application. These motors are fed with square wave currents and have trapezoidal back EMF waveform unlike the sinusoidal PMSM motors. The characteristics of these two motors are compared against the standard 3-phase dual rotor BLDC motor. They combine the positive characteristics of the dual rotor and multiphase BLDC motors, thus achieving less per phase stator current, high power and torque density, and better fault tolerance capability. The main contributions of the current paper are:

- Two new dual rotor multiphase BLDC motors as 5-, and 7-phase are designed to drive an EV. The characteristics of these motors are compared with the standard 3-phase dual rotor BLDC motor. Finite Element Method (FEM) based two-dimensional models of the motors were developed with the JMAG Designer.
- Load and no-load analysis of the three designed motors were performed.
- Fault analysis of the three motors is provided to compare their fault tolerance. Open circuit faults, high-impedance faults, and demagnetization of the permanent magnets are studied.

## II. ANALYTICAL STUDY

The main design parameters of the BLDC motor are the diameter of the armature, the stack length, and the air-gap length, through which the energy conversion process is completed. The calculation of these three design parameters is a fundamental step in any electric motor design. BLDC motor's electromagnetic loading comprises of the specific electrical loading and the specific magnetic loading. These loads define torque, efficiency, and other mechanical characteristics of the motor. Even though the motors in this study have two rotors, the design of any BLDC motor starts with the general sizing equation. The sizing equation gives the relationship between the main design parameters and the electromagnetic load of the dual-rotor BLDC motor. The main design specifications of the dual-rotor BLDC motor are derived as follows.

$$P_{em} = 11.\alpha_p.B_a.A_a.\left(\frac{D}{1000}\right)^2.\frac{L}{1000}.n_N \quad (1)$$

where $P_{em}$ is the apparent power, $L$ is the stator's stack length, $D$ is the armature's diameter, $B_a$ is the specific magnetic loading, and $A_a$ is the specific electrical load. The rated speed of the motor represented by $n_N$ and $\alpha_p$ is a constant which depends on the pole arc of the motor.

The BLDC motor having trapezoidal back EMF is modeled using the equivalent circuit shown in Figure 1. The voltage of the single phase can be derived as:

$$V_a = i_a R_a + L_a \frac{di_a(t)}{dt} + e_a \quad (2)$$

where $V_a$ is the phase voltage, $R_a$ is the phase resistance, $L_a$ is the phase inductance, $e_a$ is the generated back EMF, and $i_a$ is the phase current.

The generated back EMF and torque constant are functions of the relative rotor position. The voltage equation for multiple phases based on the back EMF is expressed as:

$$\begin{bmatrix} V_a \\ V_b \\ \vdots \\ \vdots \\ V_n \end{bmatrix} = \begin{bmatrix} R_a & 0 & \dots & 0 \\ 0 & R_b & \dots & 0 \\ \vdots & \vdots & \ddots & \vdots \\ 0 & 0 & \cdots & R_n \end{bmatrix} \begin{bmatrix} i_a \\ i_b \\ \vdots \\ \vdots \\ i_n \end{bmatrix} + \frac{d}{dt} \begin{bmatrix} i_a \\ i_b \\ \vdots \\ \vdots \\ i_n \end{bmatrix} + \begin{bmatrix} e_a \\ e_b \\ \vdots \\ \vdots \\ e_n \end{bmatrix} \quad (3)$$

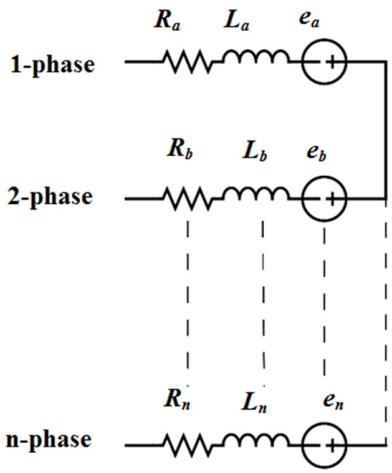


Fig. 1. Equivalent circuit of the n-phase BLDC motor.

For single phase, the expression for the current is derived as a function of supplied voltage, phase inductance, and back EMF as:

$$\frac{d}{dt} i_a = \frac{1}{3L_a}[2V_{bb} + V_{bc} - 3R_a i_a + \emptyset p w_m(-2e'_a + e'_b + e'_c)] \quad (4)$$

where $\omega_m$ is the rotational speed, $p$ is the pole pair number, and $\emptyset$ is the induced flux. The phase inductance is considered constant as the relative rotor position does not affect it. The following equation shows phase inductances BLDC motor:

$$L_a = L_{aa} - M$$
$$L_b = L_{bb} - M$$
$$\vdots$$
$$L_n = L_{nn} - M \quad (5)$$

where $M$ is the mutual inductance, $L_n$ is the phase inductance for the $n$-phase and $L_{nn}$ is the self-inductance. From (3) and (5), the equation for phase voltages can be rewritten as:

$$\begin{bmatrix} V_a \\ V_b \\ \vdots \\ V_n \end{bmatrix} = \begin{bmatrix} R_a & 0 & \dots & 0 \\ 0 & R_b & \dots & 0 \\ \vdots & \vdots & \ddots & \vdots \\ 0 & 0 & \cdots & R_n \end{bmatrix} \begin{bmatrix} i_a \\ i_b \\ \vdots \\ i_n \end{bmatrix} + \begin{bmatrix} L_a & 0 & \dots & 0 \\ 0 & L_b & \dots & 0 \\ \vdots & \vdots & \ddots & \vdots \\ 0 & 0 & \cdots & L_n \end{bmatrix} \frac{d}{dt} \begin{bmatrix} i_a \\ i_b \\ \vdots \\ i_n \end{bmatrix} + \begin{bmatrix} e_a \\ e_b \\ \vdots \\ e_n \end{bmatrix} \quad (6)$$

The back EMF of the motor depends on rotor speed, rotor relative position, magnetic field intensity, and the number of turns. For a n-phase BLDC motor, the phase angle difference is (360/$n$) for each phase of the back EMF. So, the back EMF of each phase is:

$$\begin{bmatrix} e_a \\ e_b \\ \vdots \\ e_n \end{bmatrix} = \begin{bmatrix} K_{E_n}(\theta) \\ K_{E_n}\left(\theta - \frac{2\pi}{n}\right) \\ \vdots \\ K_{E_n}\left(\theta - \frac{2\pi}{n}(n-1)\right) \end{bmatrix} . \omega \quad (7)$$

In (7), the back electromotive force constant of one phase of n-phase BLDC motor is represented by $K_{E_n}$. The per phase output torques are derived as:

$$\begin{bmatrix} T_a \\ T_b \\ \vdots \\ T_n \end{bmatrix} = \begin{bmatrix} K_{T_n}(\theta) \\ K_{T_n}\left(\theta - \frac{2\pi}{n}\right) \\ \vdots \\ K_{T_n}\left(\theta - \frac{2\pi}{n}(n-1)\right) \end{bmatrix} . \begin{bmatrix} I_a \\ I_b \\ \vdots \\ I_n \end{bmatrix}^{-1} \quad (8)$$

where $K_{T_n}$ is the torque constant of one phase of the n-phase BLDC motor. The total electromagnetic torque is given as:

$$T_e = T_a + T_b + \cdots + T_n \quad (9)$$

## III. DUAL ROTOR MULTIPHASE BLDC MOTOR DESIGN

### A. Structure of the Dual Rotor BLDC Motor

Figure 2 represents the cross-section of the 2D CAD model of a dual rotor BLDC motor. The motor consists of a stator sandwiched between two (outer and inner) rotors. The magnets of both rotors are polarized in the same direction. The flux generated by the outer magnets goes through the outer teeth of the stator and the flux driven by the inner magnets goes through the inner teeth of the stator. This structure enables the motor to have low overall volume and improved torque density. With this structure, high torque to volume ratio is obtained, which is critical for EV applications. In the designed dual-rotor multiphase BLDC motor, full-pitched concentrated windings are used. This winding configuration reduces the requirement of greater stator slot numbers and reduces the use of copper.

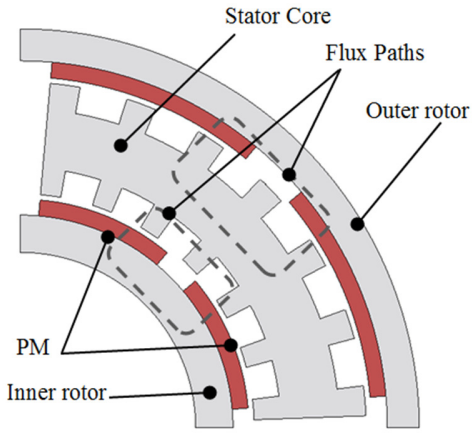


Fig. 2. Structure of the proposed dual rotor BLDC motor.

### B. Determination of Motor Power

The first step in any motor design is to determine the motor toque and the nominal speed. Two parameters define the motor dimensions, motor radius and stack length. The required power to drive the vehicle can be deduced as [21]:

$$p_{em} \geq max[p_e, p_a, p_c] \quad (10)$$

where $p_e$ is the maximum power of the motor when the vehicle achieves maximum speed, $p_a$ is the maximum power of the motor when the vehicle is at highest gradient, and $p_c$ is the maximum power of the motor when the vehicle achieves maximum acceleration. $p_e$, $p_a$ and $p_c$ are defined by (11), (12) and (13) respectively:

$$p_e = \frac{u_{max}}{360\eta_T}\left(mgf + \frac{C_D A u_m^2}{21.15}\right) \quad (11)$$

$$p_a = \frac{u_i}{360\eta_T}\left(mgf\, cos\alpha_{max} + mg\, sin\alpha_{max} + \frac{C_D A u_i^2}{21.15}\right) \quad (12)$$

$$p_c = \frac{1}{360 t_a \eta_T}\left(\delta m \frac{u_a^2}{2\sqrt{t_a}} + mgf \frac{u_a}{1.5} t_a + \frac{C_D A u_a^3}{21.15*2.5} t_a\right) \quad (13)$$

where $u_i$ is the initial velocity, $u_{max}$ is the maximum velocity, $u_a$ is the final velocity, and $\delta$ is the mass conversion coefficient of the vehicle.

The maximum speed $n_{max}$ of the motor is calculated as:

$$n_{max} = \frac{u_{max}*10^3}{120\pi r} \quad (14)$$

The nominal speed $n_N$ is related to maximum speed as:

$$n_{max} = \beta n_N \quad (15)$$

where $\beta$ is the coefficient of constant power meter. Increasing the value of $\beta$ will increase the generated torque. Its value ranges between 2 and 4. A large size power converter is needed to achieve a greater value of $\beta$.

### *C. Machine Design and Comparison*

To study the effect of different phase numbers on the performance of motors, three different BLDC (3-phase, 5-phase, and 7-phase) motors were designed. To allow a fair comparison of the three motors, similar materials were used and most of the geometric parameters were kept the same. The three motors were analyzed with FEM. Table I shows the design parameters of the three dual rotor BLDC motors. The cross sections of the simulation models for the three motors are shown in Figure 3.

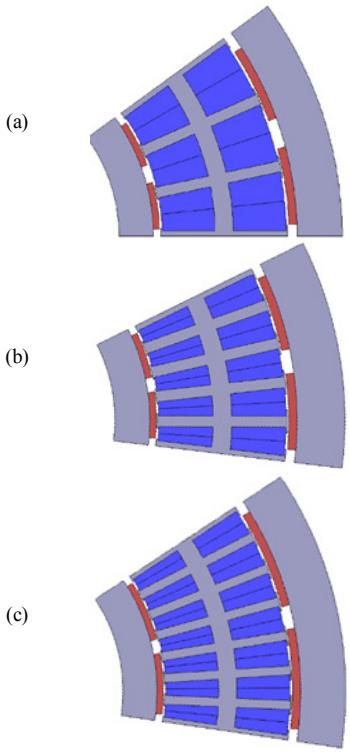


Fig. 3. Cross section of the simulation models. (a) 3-phase dual rotor motor, (b) 5-phase dual rotor motor, (c) 7-phase dual rotor motor.

TABLE I. DESIGN PARAMETERS

| Designed Motors | 3- Ph | 5- Ph | 7- Ph |
|---|---|---|---|
| Number of poles (p) | 20 | 20 | 20 |
| Number of turns | 35 | 35 | 35 |
| Number of slots | 27 | 40 | 63 |
| Outer diameter(mm) | 110 | 110 | 110 |
| Stack length (mm) | 50 | 50 | 50 |
| Current density (A/mm$^2$)) | 5 | 5 | 5 |
| Rated speed | 900rpm | 900rpm | 900rpm |
| Magnetic loading (T) | 0.8 | 0.8 | 0.8 |
| Magnets | NdFeB | NdFeB | NdFeB |

## IV. NO LOAD OPERATION

In dual rotor BLDC motor, two independent flux loops are formed in the outer and inner air gaps as displayed in Figure 1. The flux flows from one magnet in the outer rotor through the outer air gap to the teeth of the outer stator. Following the core of the outer stator, the flux flows back to the opposite polarity of the magnet and thus completes a loop. In a similar fashion, a flux loop is created in the lower air gap between the inner rotor and the stator. A different amount of flux is generated in each air gap and two independent back EMFs are generated in each stator. At no-load conditions, no current flows in the armature winding, and a magnetic field is generated by the permanent magnet. The no-load characteristics of the motor are obtained by running the motor without input current. Cogging torque is generated due to the interaction of magnets and coils at no load. The cogging torques of the three designed motors were compared. The conventional three-phase BLDC motor demonstrated a greater cogging torque as compared to the two proposed motors. Furthermore, the 7-phase dual rotor BLDC motor indicated a reduction in cogging torque than the 5-phase dual rotor BLDC motor.

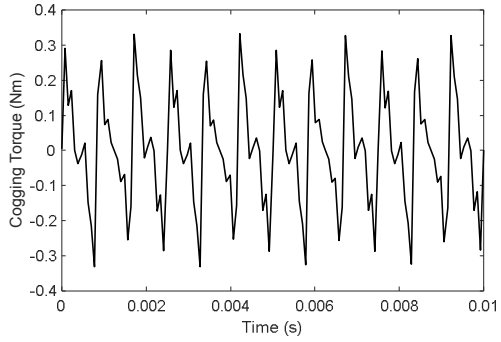


Fig. 4. Cogging torque of the 3-phase BLDC motor.

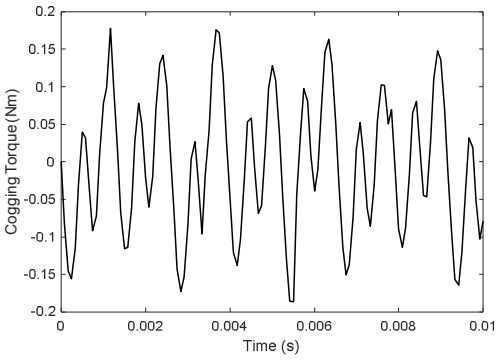


Fig. 5. Cogging torque of the 5-phase BLDC motor.

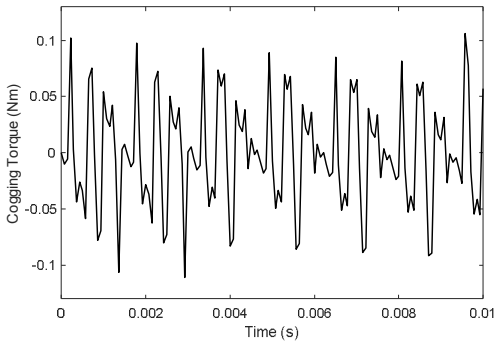


Fig. 6. Cogging torque of the 7-phase BLDC motor.

## V. LOAD OPERATION

To analyze the dual rotor multi-phase motors under load conditions, they were driven by a trapezoidal current source. A logic commutation was developed for each motor [22]. The interaction of permanent magnets and the magnetic field of the stator coils produce torque. For an n-phase dual rotor BLDC motor, one phase is positively energized, another phase is negatively energized, and the remaining phases are not energized.

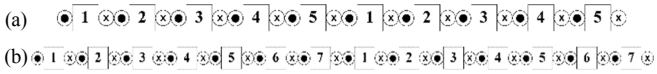


Fig. 7. Stator winding configuration: (a) 5-phase motor (b) 7-phase motor.

As shown in Figure 8, each phase of the n-phase BLDC motor is star-connected using 2n switches, where n is the number of phases. Since all three dual rotor BLDC motors are designed with the same electric and magnetic loading, the per phase rms current of the three-phase motor is the largest. As shown in Figure 9, the peak value of the 3-phase motor is 86A, of the 5-phase motor is 45A, and of the 7-phase motor is 32A.

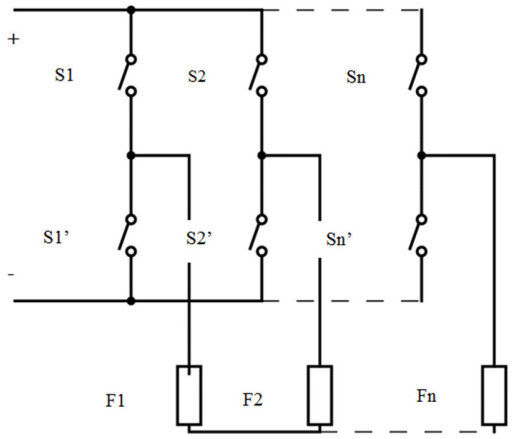


Fig. 8. Winding diagram of the n-phase BLDC motor.

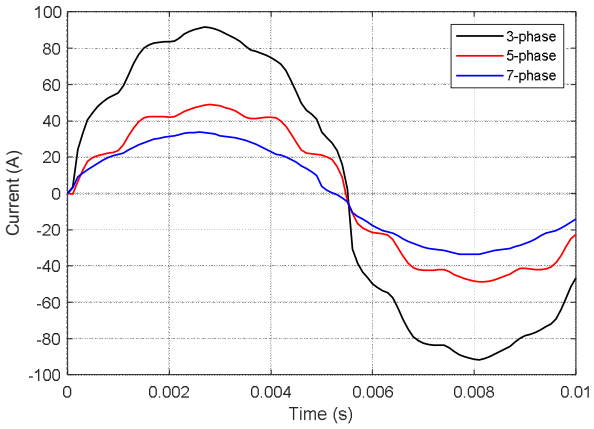


Fig. 9. Stator phase current waveforms.

Figures 10-12 show the wave forms of the steady state output electromagnetic torques of the three motors. The torque ripples of the 3-phase motor are the highest, whereas the torque ripples are reduced with increasing number of phases. However, the torque ripples of the 5-phase motor can be considered satisfactory. Hence, a phase number greater than 5 is only necessary to reduce the stator current.

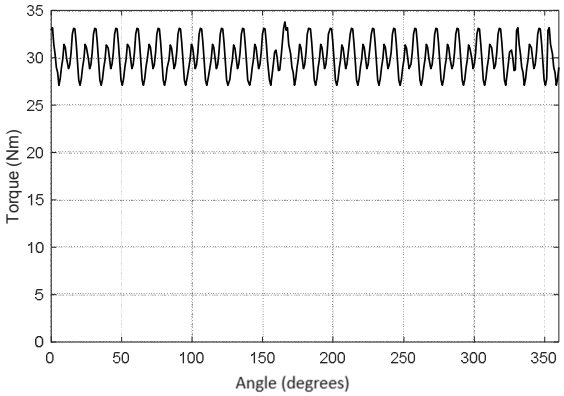


Fig. 10. Torque waveform of the 3-phase motor.

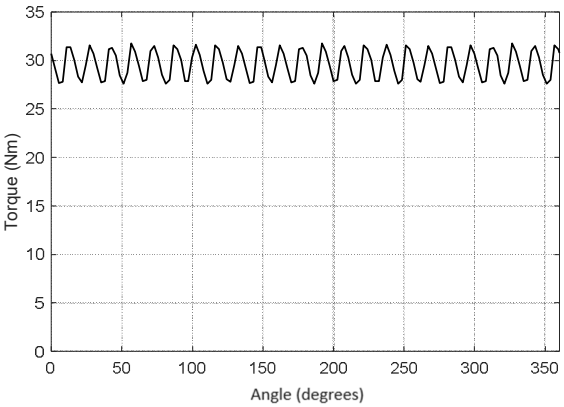


Fig. 11. Torque waveform of the 5-phase motor.

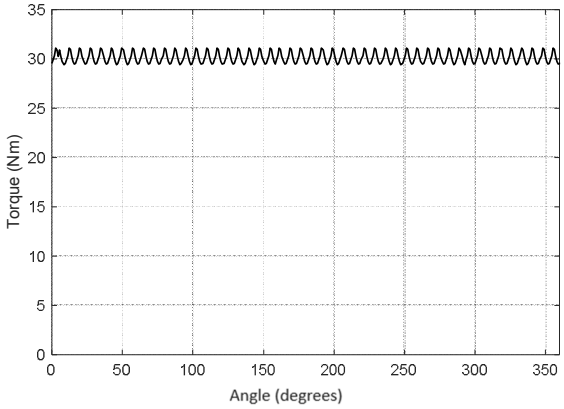


Fig. 12. Torque waveform of the 7-phase motor.

## VI. FAULT ANALYSIS

This section analyzes the transient process of the three designed dual rotor BLDC motors under various fault conditions. The performance of the three motors under various short and open circuit faults was analyzed. Figure 13 shows the comparison of the average output torque of each motor under different faults. The Figure shows either an open circuit fault or short circuit faults by phase number. To simulate these faults, a fault was introduced at certain time using switches. At the time of the fault, there was a sudden dip in the average torque and the torque ripples were increased.

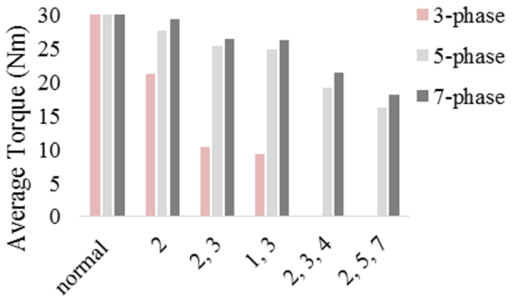


Fig. 13. Average torque under various open or short circuit fault conditions.

High impedance faults occur due to broken strands of the motor winding. The most common type is the high resistance fault. This fault was simulated using extra resistance in series with the phase winding. The value of this resistance is obtained from:

$$R_{extra} = \frac{1}{1-\sigma}(R_{inductor} + R_{end}) \quad (16)$$

where $\sigma$ defines the percentage of the broken wires. Tables II-IV compare the effect of this fault on the three motors. Increasing the phase number makes the motor more prone to broken strand faults.

TABLE II. HIGH IMPEDANCE FAULT CONDITION IN 3-PHASE MOTOR

| Condition | Average torque | Percentage of normal torque |
|---|---|---|
| Normal condition | 30 | 100% |
| 20% Broken strands | 21.708 | 72.36% |
| 35% Broken strands | 20.319 | 67.3% |
| 65% Broken strands | 14.469 | 48.23% |

TABLE III. HIGH IMPEDANCE FAULT CONDITION IN 5-PHASE MOTOR

| Condition | Average torque | Percentage of normal torque |
|---|---|---|
| Normal condition | 30 | 100% |
| 20% Broken strands | 26.41 | 88.04% |
| 35% Broken strands | 23.54818966 | 76.8% |
| 65% Broken strands | 20.15 | 67.17% |

TABLE IV. HIGH IMPEDANCE FAULT CONDITION IN 7-PHASE MOTOR

| Condition | Average torque | Percentage of normal torque |
|---|---|---|
| Normal condition | 30 | 100% |
| 20% Broken strands | 28.43 | 84.76% |
| 35% Broken strands | 26.02 | 86.73% |
| 65% Brokens strands | 23.72 | 79.06% |

Extreme temperature and high electrical loading can cause demagnetization of the BLDC motors, decreasing the average output torque. The designed motors were studied under different demagnetization conditions. When all magnets were demagnetized by 4%, the average torque decreased by 12.7%, 8.3%, and 6.6% for the 3-phase, 5-phase, and 7-phase BLDC motors respectively.

## VII. COMPARISON WITH THE AVAILABLE LITERATURE

The combination of the characteristics of the dual rotor and multiphase permanent motors is available in literature for Permanent Magnet Synchronous Motors (PMSM) [23-24]. In [23], a dual-rotor PMSM was designed, a motor with sinusoidal back EMF, to get high torque density and good fault tolerance capability. The performance and fault tolerance of the same dual-rotor five phase PMSM is investigated in [24].

To the best of our knowledge, no literature is available with regard to the dual-rotor multiphase BLDC motors. In the current research work, two dual rotor BLDC motors with 5 and 7 phases were designed for EV application. These motors were fed with square wave currents having trapezoidal back EMF waveforms unlike the sinusoidal back EMF in PMSM motors. The characteristics of the two proposed motors were compared against the standard 3-phase dual rotor BLDC motor. The designed motors have the advantages of the dual rotor and multiphase motors, thus achieving less per phase stator current, high power and torque density, and better fault tolerance capability.

## VIII. CONCLUSION

Considering the requirements of a high torque EV, two new dual rotor BLDC motors were designed and studied in this paper. The dual-rotor PM BLDC motor promises high torque density and high efficiency. This machine consists of an inner rotor, an outer rotor, and a stator between the two rotors. Three motors: 3-phase, 5-phase, and 7-phase have been designed and FEM was utilized to analyze their performance. The main design parameters and materials are preliminarily decided by standard methods. Analytical modeling of the multiphase BLDC motor has been presented. The performance of the 5- and 7-phase dual rotor BLDC motors has been evaluated under load and no-load conditions and the results were compared with the standard 3-phase dual rotor BLDC motor.

To allow a fair comparison, most of the design parameters and operating conditions of the motors were kept the same with the ones of the base motor. The number of stator slots for each motor has been determined by the phase number. The cogging torque and back EMF waveforms were obtained at no load. Average torque and stator current waveforms were obtained at loaded conditions. The results show that increasing the phase number decreases phase current. This enables the use of low rating power electronic switches. The output torque can also be increased per RMS current for the same volume of the motor. Torque ripples also decreased as the number of phases increased. Finally, fault analysis of the three motors has been performed to analyze their performance under fault conditions. It was found that the increased phase number makes the motor more fault tolerant and increases reliability.

## REFERENCES


[1] P. Zheng, Y. Liu, Y. Wang, and S. Cheng, "Magnetization analysis of the brushless DC motor used for hybrid electric vehicle," *IEEE Transactions on Magnetics*, vol. 41, no. 1, pp. 522–524, Jan. 2005, https://doi.org/10.1109/TMAG.2004.838746.

[2] J. A. Sanguesa, V. Torres-Sanz, P. Garrido, F. J. Martinez, and J. M. Marquez-Barja, "A Review on Electric Vehicles: Technologies and Challenges," *Smart Cities*, vol. 4, no. 1, pp. 372–404, Mar. 2021, https://doi.org/10.3390/smartcities4010022.

[3] K. T. Chau, C. C. Chan, and C. Liu, "Overview of Permanent-Magnet Brushless Drives for Electric and Hybrid Electric Vehicles," *IEEE Transactions on Industrial Electronics*, vol. 55, no. 6, pp. 2246–2257, Jun. 2008, https://doi.org/10.1109/TIE.2008.918403.

[4] W. Cai, X. Wu, M. Zhou, Y. Liang, and Y. Wang, "Review and Development of Electric Motor Systems and Electric Powertrains for New Energy Vehicles," *Automotive Innovation*, vol. 4, no. 1, pp. 3–22, Feb. 2021, https://doi.org/10.1007/s42154-021-00139-z.

[5] A. Eldho Aliasand and F. T. Josh, "Selection of Motor foran Electric Vehicle: A Review," *Materials Today: Proceedings*, vol. 24, pp. 1804–1815, Jan. 2020, https://doi.org/10.1016/j.matpr.2020.03.605.

[6] T. A. Zarma, A. A. Galadima, and M. A. Aminu, "Review of Motors for Electric Vehicles," *Journal of Scientific Research and Reports*, pp. 1–6, Oct. 2019, https://doi.org/10.9734/jsrr/2019/v24i630170.

[7] M. Yildirim, H. Kurum, D. Miljavec, and S. Corovic, "Influence of Material and Geometrical Properties of Permanent Magnets on Cogging Torque of BLDC," *Engineering, Technology & Applied Science Research*, vol. 8, no. 2, pp. 2656–2662, Apr. 2018, https://doi.org/10.48084/etasr.1725.

[8] Z. Q. Zhu and D. Howe, "Electrical Machines and Drives for Electric, Hybrid, and Fuel Cell Vehicles," *Proceedings of the IEEE*, vol. 95, no. 4, pp. 746–765, Apr. 2007, https://doi.org/10.1109/JPROC.2006.892482.

[9] T.-Y. Lee, M.-K. Seo, Y.-J. Kim, and S.-Y. Jung, "Motor Design and Characteristics Comparison of Outer-Rotor-Type BLDC Motor and BLAC Motor Based on Numerical Analysis," *IEEE Transactions on Applied Superconductivity*, vol. 26, no. 4, pp. 1–6, Jun. 2016, https://doi.org/10.1109/TASC.2016.2548079.

[10] M. Dahbi, S. Doubabi, A. Rachid, and D. Oulad-Abbou, "Performance evaluation of electric vehicle brushless direct current motor with a novel high-performance control strategy with experimental implementation," *Proceedings of the Institution of Mechanical Engineers, Part I: Journal of Systems and Control Engineering*, vol. 234, no. 3, pp. 358–369, Mar. 2020, https://doi.org/10.1177/0959651819854562.

[11] Y. Li, D. Bobba, and B. Sarlioglu, "Design and Optimization of a Novel Dual-Rotor Hybrid PM Machine for Traction Application," *IEEE Transactions on Industrial Electronics*, vol. 65, no. 2, pp. 1762–1771, Feb. 2018, https://doi.org/10.1109/TIE.2017.2739686.

[12] B. V. R. Kumar and K. S. Kumar, "Design of a new Dual Rotor Radial Flux BLDC motor with Halbach array magnets for an electric vehicle," in *International Conference on Power Electronics, Drives and Energy Systems*, Trivandrum, India, Dec. 2016, pp. 1–5, https://doi.org/10.1109/PEDES.2016.7914552.

[13] Y.-H. Yeh, M.-F. Hsieh, and D. G. Dorrell, "Different Arrangements for Dual-Rotor Dual-Output Radial-Flux Motors," *IEEE Transactions on Industry Applications*, vol. 48, no. 2, pp. 612–622, Mar. 2012, https://doi.org/10.1109/TIA.2011.2180495.

[14] A. Dalal and P. Kumar, "Design, Prototyping, and Testing of a Dual-Rotor Motor for Electric Vehicle Application," *IEEE Transactions on Industrial Electronics*, vol. 65, no. 9, pp. 7185–7192, Sep. 2018, https://doi.org/10.1109/TIE.2018.2795586.

[15] P. Pisek, B. Stumberger, T. Marcic, and P. Virtic, "Design Analysis and Experimental Validation of a Double Rotor Synchronous PM Machine Used for HEV," *IEEE Transactions on Magnetics*, vol. 49, no. 1, pp. 152–155, Jan. 2013, https://doi.org/10.1109/TMAG.2012.2220338.

[16] G. Boztas, M. Yildirim, and O. Aydogmus, "Design and Analysis of Multi-Phase BLDC Motors for Electric Vehicles," *Engineering, Technology & Applied Science Research*, vol. 8, no. 2, pp. 2646–2650, Apr. 2018, https://doi.org/10.48084/etasr.1781.

[17] M. Salehifar, R. S. Arashloo, J. M. Moreno-Equilaz, V. Sala, and L. Romeral, "Fault Detection and Fault Tolerant Operation of a Five Phase PM Motor Drive Using Adaptive Model Identification Approach," *IEEE Journal of Emerging and Selected Topics in Power Electronics*, vol. 2, no. 2, pp. 212–223, Jun. 2014, https://doi.org/10.1109/JESTPE.2013.2293518.

[18] L. Parsa and H. A. Toliyat, "Five-phase permanent-magnet motor drives," *IEEE Transactions on Industry Applications*, vol. 41, no. 1, pp. 30–37, Jan. 2005, https://doi.org/10.1109/TIA.2004.841021.

[19] H. Lu, J. Li, R. Qu, D. Ye, and Y. Lu, "Fault-Tolerant Predictive Control of Six-Phase PMSM Drives Based on Pulsewidth Modulation," *IEEE Transactions on Industrial Electronics*, vol. 66, no. 7, pp. 4992–5003, Jul. 2019, https://doi.org/10.1109/TIE.2018.2868264.

[20] E. Levi, "Multiphase Electric Machines for Variable-Speed Applications," *IEEE Transactions on Industrial Electronics*, vol. 55, no. 5, pp. 1893–1909, May 2008, https://doi.org/10.1109/TIE.2008.918488.

[21] Y. Yuan, W. Meng, X. Sun, and L. Zhang, "Design Optimization and Analysis of an Outer-Rotor Direct-Drive Permanent-Magnet Motor for Medium-Speed Electric Vehicle," *World Electric Vehicle Journal*, vol. 10, no. 2, Jun. 2019, Art. no. 16, https://doi.org/10.3390/wevj10020016.

[22] C. Oprea, C. Martis, and B. Karoly, "Six-phase brushless DC motor for fault tolerant electric power steering systems," in *International Aegean Conference on Electrical Machines and Power Electronics*, Bodrum, Turkey, Sep. 2007, pp. 457–462, https://doi.org/10.1109/ACEMP.2007.4510543.

[23] Y. Li, J. Zhao, Z. Chen, and X. Liu, "Investigation of a Five-Phase Dual-Rotor Permanent Magnet Synchronous Motor Used for Electric Vehicles," *Energies*, vol. 7, no. 6, pp. 3955–3984, Jun. 2014, https://doi.org/10.3390/en7063955.

[24] J. Zhao, X. Gao, B. Li, X. Liu, and X. Guan, "Open-Phase Fault Tolerance Techniques of Five-Phase Dual-Rotor Permanent Magnet Synchronous Motor," *Energies*, vol. 8, no. 11, pp. 12810–12838, Nov. 2015, https://doi.org/10.3390/en81112342.